Remote Vegetation Diagnostics in Ghana with a Hyperspectral Fluorescence Lidar

Rabbi Boateng, Andrew Atiogbe Huzortey, Yatana Adolphe Gbogbo, Assoumou saint-doria Yamoa, Jérémie T. Zoueu, Mikkel Brydegaard, Benjamin Anderson, and Hampus Månefjord

***Abstract*—Spectral imaging and lidar methods for the characterization of vegetation are vital for understanding plants and, in turn, food security, biodiversity, and vegetation health in a changing climate. While novel hyperspectral imaging, canopy lidar, and solar-induced fluorescence provide details on species, state, structure, and plant physiology, such data come from different instruments. Thus, post-processing and data fusion struggles with synchronization, spatial overlap, and resolution issues. Especially in the tropical regions of sub-Saharan Africa, these complex, expensive, and bulky instruments remain inaccessible. Here, in Ghana, we have built a low-cost, lightweight, and realistic instrument for simultaneously acquiring hyperspectral data of vegetation fluorescence and canopy structure with perfect spatial overlap. In this paper, we demonstrate the application of the hyperspectral fluorescence lidar for diagnostics and species specificity of locally significant crops. We demonstrate simultaneous range and fluorescence measurements of forest canopy, conducted in full sunlight. Our results indicate that the upper side of the leaves shows a more substantial deviation for stressed plants, while the lower side shows greater contrast for plant species. This new and simple tool provides a combined method for hyperspectral classification and assessment of the physiological state while also reporting the vegetation height over ground and its diversity.**

***Index Terms*—Scheimpflug lidar, low-cost instrumentation, 3D-printed instrumentation, canopy profiling, agriculture monitoring, food crops, cash crops, africa, tropics.**

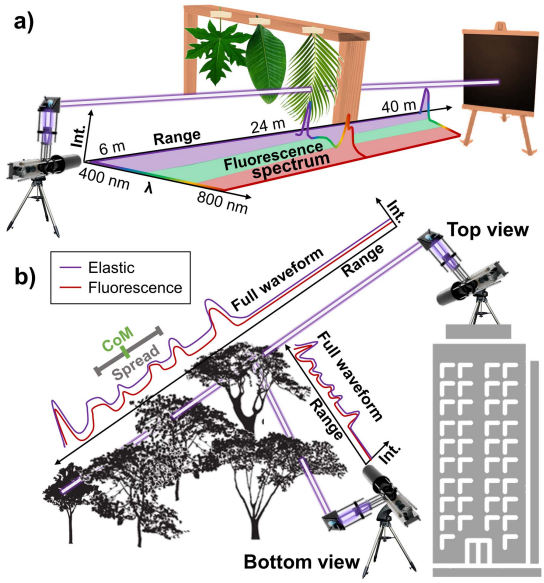

Fig. 1. a) Chlorophyll fluorescence spectra fluorescence of leaves from locally important food crops was remotely acquired. b) Canopy structure was mapped at the base and the top of the Sam Jonah library UCC campus.

I. Introduction

In a changing climate, monitoring vegetation health and stress levels ensure a proactive and resilient approach to combating threats to food security, biodiversity, and vegetation health. Food security in the African tropics is highly dependent on the health state of local food crops and plantations [1], [2]. The health states of plants are connected to specific spectral features of the reflected light from the vegetation. Plant water content [3], nitrogen fertilization estimations [4], [5], and plant vitality [6] are all features that can be monitored by, e.g., the shape and position of the red edge [7] in the reflected spectrum. Reducing the dimensionality of the spectra to vegetation indices that can be compared across studies is another predominant approach, e.g., with the normalized difference vegetation index NDVI [8], [9].

Vegetation fluorescence is linked to chlorophyll photosynthesis efficiency and carbon assimilation and can indicate stress early [10], [11], [12]. Furthermore, the spectral signature can be used for species classification [13]. The fluorescence signature is also reported to vary depending on the part of the leaf [14], which is relevant for the measurement geometry's impact on the gathered fluorescence data. The canopy structure and biomass height distribution are other important measures linked with both photosynthesis activity [15] and with biodiversity [16], [17], even including animal richness [18].

Manuscript received 30 September 2022; revised 8 December 2022; accepted 30 December 2022. Date of publication 3 January 2023; date of current version 6 February 2023. This work was supported in part by the Swedish Research Council under Grant 2018-04073 and partially funded by the Swedish International Development Agency (SIDA) through the International Science Program (ISP, Uppsala) by a grant to the African Spectral Imaging Network (AFSIN). *(Corresponding author: Hampus Månefjord.)*

Rabbi Boateng, Andrew Atiogbe Huzortey, and Benjamin Anderson are with the Laser and Fibre Optics Centre, Univeristy of Cape Coast, Cape Coast CC167, Ghana (e-mail: rabbi.boateng@stu.ucc.edu.gh; andrew.huzortey@stu.ucc.edu.gh; banderson@ucc.edu.gh).

Yatana Adolphe Gbogbo, Assoumou saint-doria Yamoa, and Jérémie T. Zoueu are with the Institut National Polytechnique Félix Houphouët-Boigny Yamoussoukro, Yamoussoukro BP 1093, Côte d'Ivoire (e-mail: yatana.gbogbo18@inphb.ci; assoumou.yamoa21@inphb.ci; jeremie.zoueu@inphb.ci).

Mikkel Brydegaard is with the Department of Physics, Lund University, SE-22100 Lund, Sweden, and also with the Norsk Elektro Optikk A/S, 0667 Oslo, Norway (e-mail: mikkel.brydegaard@fysik.lth.se).

Hampus Månefjord is with the Department of Physics, Lund University, SE-22100 Lund, Sweden (e-mail: hampus.manefjord@forbrf.lth.se).

Color versions of one or more figures in this article are available at https://doi.org/10.1109/JSTQE.2023.3234022.

Digital Object Identifier 10.1109/JSTQE.2023.3234022

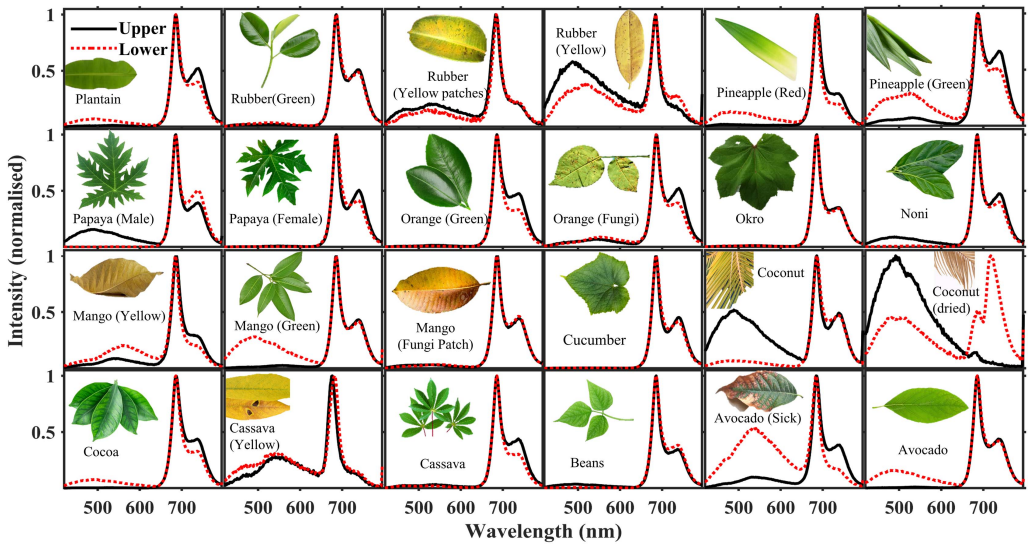

Fig. 2. The upper and lower side of each leaf was scanned remotely. There is a significant variation in the relative intensity of the blue-green fluorescence peak below 650 nm. The intensities at the red-NIR 690 and 740nm double peak also vary between species, health status, and the probed side of the leaves.

Optical methods for vegetation monitoring can be classified as elastic- and inelastic techniques, where the former probes reflected light and the latter retrieves the fluorescence. Methods are also classified as passive or active, where passive methods typically use sunlight, and active methods use an artificial light source.

Elastic passive monitoring can separate the photon energy of the reflected sunlight with hyperspectral imaging techniques, which can probe wavelengths ranging from visible through near-infrared (NIR) into short-wave infrared (SWIR), depending on the application. Visible light can, e.g., be used for detecting plant stress [19]. The relative intensity in far-red and near-infrared gives the NDVI [8], which indicates the presence of chlorophyll. For probing water content, the SWIR water absorption lines at 1.2 and 1.5μm are typically used [3], [20]. The excellent photon economy associated with sunlight enables passive vegetation mapping from global coverage, with systems mounted on satellites, to mapping individual forests or plantations with airplanes and drones [21]. These systems do, however, lack canopy-depth profiling abilities.

Active elastic canopy lidar techniques have been developed for forest characterization [22], [23], [24], [25]. These methods typically record a few discrete lidar echoes [26] and then calculate the statistical distribution of the biomass. There are also full waveform lidars that can map the complete distribution of biomass [27]. Since these lidars are typically monochromatic, there are efforts to fuse the lidar range data of the canopy structure with hyperspectral images [28], [29]. Such ventures have to handle either synchronized equipment or laborious data stitching while post-processing the data. Some multispectral lidars have been implemented through beam splitters and photomultiplier tubes (PMTs) for simultaneous canopy structure and spectral analysis [30], [31], [32]. These do, however, have limited spectral coverage. Furthermore, elastic measurements of randomly angled leaf blades are reported to suffer from incidence angle effects when the spatial resolution is on the single leaf level [33]. These effects might be avoided by instead measuring the omnidirectionally emitted fluorescence.

Passive inelastic methods to probe solar-induced fluorescence (SIF) utilize the otherwise dark Fraunhofer lines in solar radiation, where vegetation fluorescence can be assessed at these specific wavelengths [34]. Fluorescence measurements complement elastic counterparts by directly measuring photosynthetic efficiency, biomass production, and carbon assimilation [11], [12]. Due to its passive nature, SIF can be accomplished on a large scale, but the technique is technically challenging to implement.

Active and inelastic hyperspectral lidars could simultaneously resolve spectral signatures, laser-induced fluorescence (LIF), and the canopy structure without any data stitching. Reports of such instruments are rare. There are some examples of multispectral implementations using PMTs and analyzing the elastic echo for ranging [35]. Full waveform hyperspectral implementations also exist in a few examples of Scheimpflug lidars for vegetation [36], [37] and fluorescence tagging aquatic fauna [38] and insects [39].

We have replicated a 3D-printed hyperspectral fluorescence lidar [39] and used it to demonstrate simultaneous high-resolution fluorescence and ranging of locally significant food crops in Ghana. We explore specificity and health assessment of plants using the fluorescence spectra and discern whether probing the upper or lower (adaxial or abaxial) part of the leaf should be preferred. The measurements are partially conducted in full sunlight.

II. Instrumentation and Measurement Geometry

A hyperspectral lidar designed for fluorescence measurements detailed in [39] was built on the measurement site at Laser and Fibre Optics Centre (LAFOC) at the University of Cape Coast (UCC) in Ghana with the help of a 3D printer and commercial off-the-shelf components. The lidar emits a 1W,

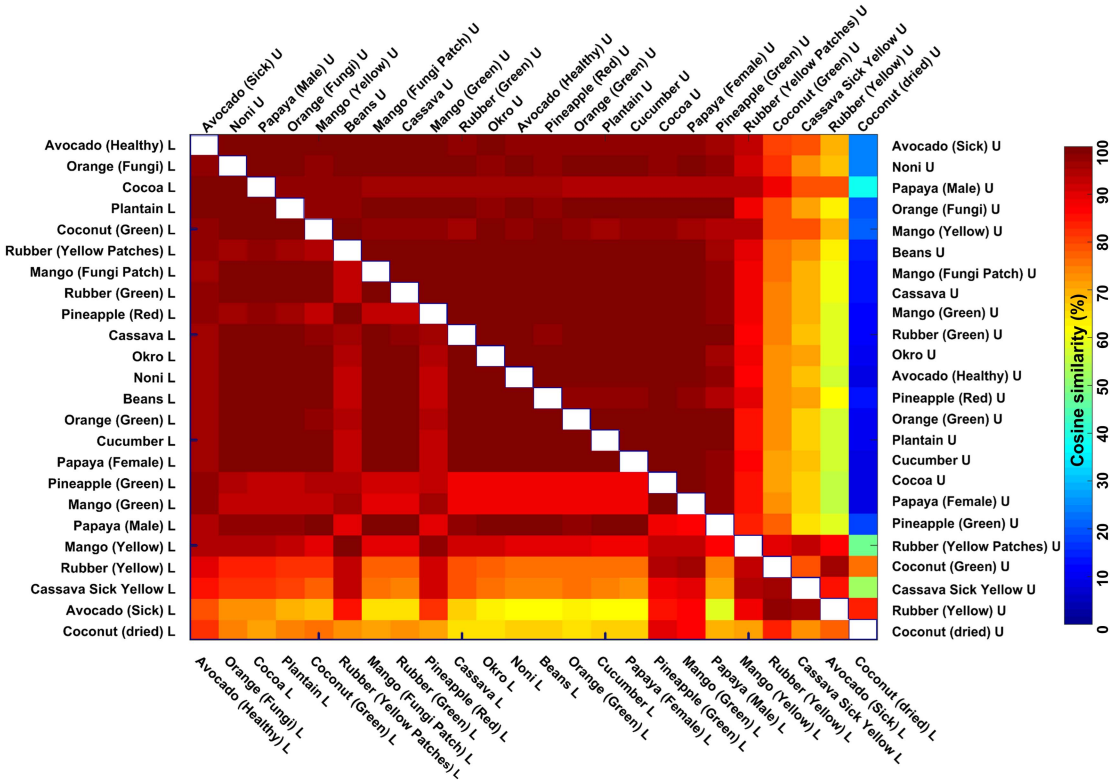

Fig. 3. The cosine similarity of the spectra of the leaves in Fig. 2. The spectra from each leaf's upper sides (denoted U) are compared in the top right triangle of the matrix. The leaves lower sides (denoted L) are correspondingly compared in the bottom left triangle. The species are sorted in decreasing similarity. The similarity of the spectra between the healthy species for the lower side is 96% compared to 98% of the upper side. The spectral similarity between different health states is on the other hand 60% for the upper side and 84% for the lower side.

Ø1", violet 405 nm laser beam. The divergence is 0.4 mrad and −0.15 mrad in the transversal and baseline axis respectively. It captures returning light in 12 bits on a camera sensor. Wavelengths from ∼390 to ∼810 nm are resolved with 70 effective spectral bands. Synchronized lock-in detection is implemented with a maximum sample and modulation frequency of 124 Hz. This is accomplished by switching laser on and off for odd and even exposures [40], [41]. The range information is acquired by triangulation and Scheimpflug configuration and spans from 6 to 120 m with 1920 range bins resulting in a relative range accuracy of 5-10%. A longpass filter was used in most applications for suppressing the elastic 405 nm signal. Some ghost effects from unfiltered elastic light were seen on the sensor when the filter was not in place.

Leaves of 15 different locally important food- and cash crops were harvested. Nine other leaves with varying sex and health states, such as dry, discolored, or fungal-infected, were also collected. The harvested leaves were stored in a humid dark box at room temperature for aeration and dark adaptation. They were transported to the laboratory for measurement on the same day. The leaves were mounted 24 m from the lidar and then scanned on their upper and lower sides to acquire the fluorescence spectra remotely (see Fig. 1(a)).

The lidar was also tested atop a building near a forest patch with seven tree species to investigate the canopy structure. The beam diameter of $\sim 5\text{cm}^2$ is comparable to and smaller than many canopy features. Hence, a single lidar exposure probes a single leaf or branch and, *per se,* does not give complete range statistics. Such metrics will instead result from scanning a forest patch by sweeping the beam across the canopy. The lidar was mounted on a motorized tripod which could change the observation angle. A top-view scan was performed from the vantage point by angling the lidar ∼45° downward. Consequently, the tripod altitude angle was continually swept with a constant angular velocity of 0.53 °/s, acquiring a signal from different parts of the canopy over time with lock-in detection. The lidar was then placed on the ground for a similar bottom-view raster scan of the same canopy, centered around approximately 45° upward, see Fig. 1(b). Measurements were taken during both day- and nighttime; daytime fluorescence measurement being very challenging due to the competition with the sunlight. Exposure times of 10 and 25 ms and gain of 15 and 24 dB were used for the day and nighttime scans, respectively. The camera sensor employed 4x4 pixel binning along the spectral and range axes. The individual spectra of the leaves in the latter canopy experiment were also acquired according to the methodology in Fig. 1(a).

III. Specificity and Diagnostics of Single Leaves

The fluorescence spectra of the leaves can be seen in Fig. 2. Of note is the relative intensity of the blue-green fluorescence band below 650 nm and the two far-red and NIR peaks at 690

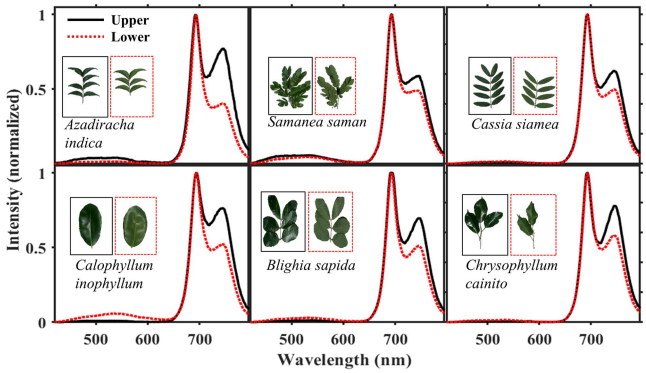

Fig. 4. Spectra from the upper and lower sides of the leaves of the tree species present in the canopy structure scan.

and 740 nm. These intensities vary among species, health status, sex, and side of the leaf probed.

The pairwise cosine similarity of each spectrum is presented in Fig. 3. where the upper side of the leaves and the lower side are compared separately. This metric was chosen for its simplicity, insensitivity to absolute signal strength, and resulting values being bounded from 0 to 100% similarity. Although we see differences in the spectra of the leaves, the reported cosine similarity is generally high for most healthy species, indicating that specificity could be challenging to probe solely based on fluorescence measurements. The coconut palm stands out with a unique spectrum, which seems reasonable to the authors due to its long distance in the phylogenetic tree to the other investigated plants. The yellow and dried leaves were also drastically different, as indicated in the right-most columns in Fig. 3. From our results, it can be concluded that for specificity, the lower side of the leaves is slightly more efficient to probe with an average cosine similarity of 96% compared to 98% of the upper side. On the other hand, the upper side is preferred for diagnosis of the health state, with an average cosine similarity of 64% compared to 80%.

The blue-green and the far red-NIR spectral features were individually compared by performing cosine similarity analysis while limiting the spectra below and above 650 nm. The most prominent species contrast was found in the blue-green spectral region

IV. Profiling of Vegetation Structures

Spectra from six of the seven species in the forest patch are presented in Fig. 4; the additional specie in the patch is the female papaya, which is presented in Fig. 2.

A scan of the Papaya tree in the canopy is compared with a scan of the other six species in Fig. 5. Panels a) and e) show photos of the two scans being taken. Panels b), c), f), and g) show the spectral shape over time for the two cases. Finally, in panels d) and h), the measured spectra at each exposure of the scans are compared to each species' known spectra, of the corresponding side of the leaves, thus estimating the possibility of doing remote classification of specie using the remote fluorescence signature. In d), the scan of the papaya consistently has a higher cosine

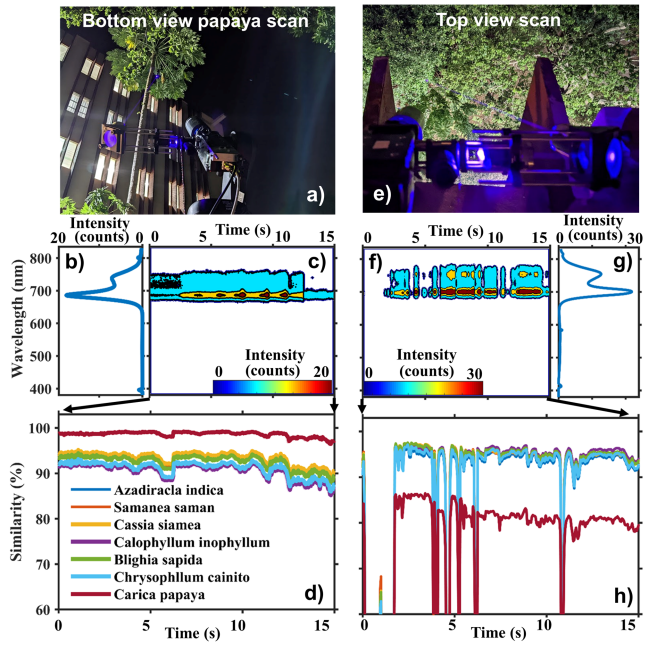

Fig. 5. Panels a) to d) all correspond to the bottom view scanning of the female Carcia papaya, while e) to h) correspond to scanning the other six species from a top view. a) and e) are photos of the scan position. Panels c) and f) Show the wavelength-time contour plot of the 15 s scans. The average intensity over the range was used. The 15 s scans correspond to sweep angles of 8°. b) and g) Show the corresponding average spectra during the scans. Finally, d) and h) show the cosine similarity of the captured spectra at each exposure compared to the spectra of the known species in the canopy. When the trees' branches or stem are probed rather than the leaves, the similarity to all species drop, as seen in h) for some exposures.

similarity to the papaya spectrum. Meanwhile, in panel h) the cosine similarity is higher for the other six species scanned. It is not, however, possible to distinguish which exact specie is scanned in the latter case.

The simultaneous range- and wavelength data from a daytime and a nighttime vegetation scan are shown in Fig. 6. Here, the mean intensity in all ranges and wavelengths are shown for both scans. Range statistics in the form of center of mass (CoM), spread, skewness, and kurtosis were calculated for both canopy scans. These are known as the first four statistical moments; the former two are gauged in meters while the latter two are unitless. The nighttime scan had $CoM = 23$ m, spread $= 4.4$ m, skewness $= 3.5$, and kurtosis $= 72$. The daytime scan had $CoM = 24$ m, spread $= 11$ m, skewness $= 4.3$, and kurtosis $= 38$. Note that these measurements are indeed taken of the same forest patch but not the same angles; hence, we do not expect the same canopy statistical values. The range axes do not correspond to vegetation height but actual range from the lidar. Had the scans been performed in zenith or nadir configuration on, e.g., a drone, the more relevant and comparable height distribution could be acquired. Alternatively, knowledge of scan angle could provide vegetation height distribution after post-processing the data. The daytime data in Fig. 6(b). contains more noise than the nighttime counterpart because a shorter exposure time and lower gain had to be used to not get saturated signal from the competing sunlight.

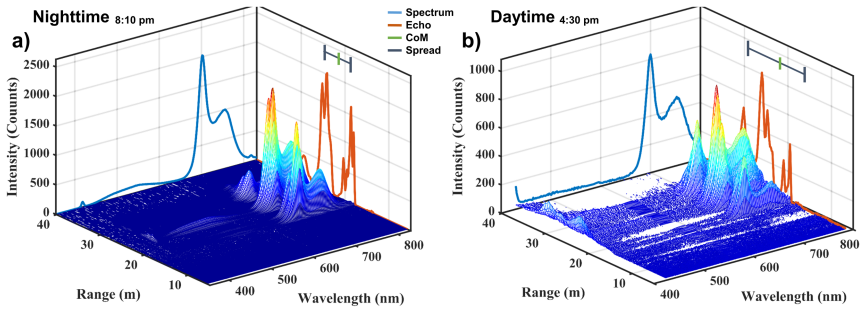

Fig. 6. a) A daytime and b) nighttime top view scan of the forest canopy. The intensity in average counts is shown for the wavelength and range of the scan. The maximum of the fluorescence spectrum is outlined in blue at the plane of 40m range. Similarly, at the plane of 800 nm wavelength, the full range echo is outlined in orange together with an indicator of the center of mass (CoM) and the spread of the range echo.

V. Discussion and Outlook

We have built a lightweight, low-cost hyperspectral lidar for vegetation fluorescence application based on the novel concepts reported in [39]. The instrument is deployed in Ghana in the low-income and tropical region of sub-Saharan Africa, and we use it to address local applications of vegetation and agriculture. An instrument that simultaneously maps spectrum and full waveform range information combines relevant information usually gathered from multiple instruments without data fusion issues. We did, however, notice some ghost effects of elastic light on the lidar sensor when the longpass filter was not used. Thus the spectra in Figs. 2, 4, and 6(b) had a ghost peak removed at around 600 nm.

We achieve instant synchronization of spectral and ranging data by acquiring both with the same exposure as opposed to typical multispectral elastic lidar for vegetation [42]. We demonstrate the ability to acquire vegetation fluorescence during darkness and in full sunlight. Measurements in full sunlight are technically challenging due to a high background signal but are highly relevant for probing diurnal variations of vegetation fluorescence [43]. The lock-in detection for noise suppression can struggle with continuous angular sweeps, as in our examples, especially with relatively slow sample rates and an irregular target as a forest canopy. Implementations to stop the sweep between each background subtraction could also be explored to increase the signal-to-noise level. With a continuous sweep, will the subtracted background not correspond to the position of the illuminated measurement one exposure earlier. Hence, background subtraction works better for slow angular velocities and short exposure times. Whereas fast angular velocity and short exposure times minimize the effects of fluorescence saturation and kinetics. Fluorescence saturation and kinetics can distort or enrich the acquired data depending on whether it is considered in the design of the measurement geometry and subsequent data processing. The saturation pulse method can, e.g., be used to detect plant stress [44], and fluorescence kinetics can, e.g., be utilized to tackle otherwise challenging tasks such as discriminating the sex of nutmeg trees [45].

Our results comparing the leaves' upper and lower sides indicate that a top view might be preferred for health assessment while a bottom view might be preferred for species classification. As reported in [14] the leaves' different sides produce distinct spectra, which remain unexplored in recent vegetation monitoring studies. The compact size of our hyperspectral lidar enables vegetation mapping on a larger scale than in this study, with the lidar mounted on a drone or carried in a rucksack. Such an experiment, with our lidar system, would yield valuable information on the biomass height distribution in addition to the fluorescence signatures of the canopies.

Among the investigated species, the fluorescence spectra alone do not seem to suffice to accomplish precise classification of tree species. Increased specificity could possibly be achieved with data processing using, e.g., spectral band ratios [10], [46], singular value decomposition (SVD) coupled with hierarchical clustering [37], or machine learning methods [47], [48].

Acknowledgment

We want to thank all participants in the workshop at UCC where this instrument was built and the measurements were taken, including Moses Jojo Eghan, Peter Osei-Wusu Adueming, Jerry Opoku-Ansah, Charles Lloyd Yeboah Amuah, and the UCC Library Management.

References

[1] S. Dercon and D. Gollin, "Agriculture in African development: A review of theories and strategies," CSAE Working Paper Series 2014-22, Centre Study Afr. Econ., Univ. Oxford, 2014.
[2] P. P. Kurukulasuriya et al., "Will African agriculture survive climate change?," *World Bank Econ. Rev.*, vol. 20, no. 3, pp. 367–388, 2006.
[3] D. A. Sims and J. A. Gamon, "Estimation of vegetation water content and photosynthetic tissue area from spectral reflectance: A comparison of indices based on liquid water and chlorophyll absorption features," *Remote Sens. Environ.*, vol. 84, no. 4, pp. 526–537, 2003.
[4] J. McMurtrey Iii et al., "Distinguishing nitrogen fertilization levels in field corn (Zea mays L.) with actively induced fluorescence and passive reflectance measurements," *Remote Sens. Environ.*, vol. 47, no. 1, pp. 36–44, 1994.
[5] Y. Zhu et al., "Analysis of common canopy reflectance spectra for indicating leaf nitrogen concentrations in wheat and rice," *Plant Prod. Sci.*, vol. 10, no. 4, pp. 400–411, 2007.
[6] F. Boochs et al., "Shape of the red edge as vitality indicator for plants," *Remote Sens.*, vol. 11, no. 10, pp. 1741–1753, 1990.
[7] M. A. Cho and A. K. Skidmore, "A new technique for extracting the red edge position from hyperspectral data: The linear extrapolation method," *Remote Sens. Environ.*, vol. 101, no. 2, pp. 181–193, 2006.
[8] J. Xue and B. Su, "Significant remote sensing vegetation indices: A review of developments and applications," *J. Sensors*, vol. 2017, pp. 1–17, 2017.

[9] A. Vrieling, K. M. de Beurs, and M. E. Brown, "Variability of African farming systems from phenological analysis of NDVI time series," *Climatic Change*, vol. 109, no. 3, pp. 455–477, 2011.

[10] G. H. Krause and E. Weis, "Chlorophyll fluorescence and photosynthesis: The basics," *Annu. Rev. Plant Biol.*, vol. 42, no. 1, pp. 313–349, 1991.

[11] M. Meroni et al., "Remote sensing of solar-induced chlorophyll fluorescence: Review of methods and applications," *Remote Sens. Environ.*, vol. 113, no. 10, pp. 2037–2051, 2009.

[12] P. E. Campbell et al., "Contribution of chlorophyll fluorescence to the apparent vegetation reflectance," *Sci. Total Environ.*, vol. 404, no. 2-3, pp. 433–439, 2008.

[13] L. Longchamps et al., "Discrimination of corn, grasses and dicot weeds by their UV-induced fluorescence spectral signature," *Precis. Agriculture*, vol. 11, no. 2, pp. 181–197, 2010.

[14] U. Schreiber, R. Fink, and W. Vidaver, "Fluorescence induction in whole leaves: Differentiation between the two leaf sides and adaptation to different light regimes," *Planta*, vol. 133, no. 2, pp. 121–129, 1977.

[15] B. Dechant et al., "Canopy structure explains the relationship between photosynthesis and sun-induced chlorophyll fluorescence in crops," *Remote Sens. Environ.*, vol. 241, 2020, Art. no. 111733.

[16] H. T. Ishii, S. Tanabe, and T. Hiura, "Exploring the relationships among canopy structure, stand productivity, and biodiversity of temperate forest ecosystems," *Forest Sci.*, vol. 50, no. 3, pp. 342–355, 2004.

[17] L. Pesola et al., "Linking above-ground biomass and biodiversity to stand development in urban forest areas: A case study in Northern Italy," *Landscape Urban Plan.*, vol. 157, pp. 90–97, 2017.

[18] A. B. Davies and G. P. P. Asner, "Advances in animal ecology from 3D-LiDAR ecosystem mapping," *Trends Ecol. Evol.*, vol. 29, no. 12, pp. 681–691, 2014.

[19] J. Behmann, J. Steinrücken, and L. Plümer, "Detection of early plant stress responses in hyperspectral images," *ISPRS J. Photogrammetry Remote Sens.*, vol. 93, pp. 98–111, 2014.

[20] C. M. Champagne et al., "Validation of a hyperspectral curve-fitting model for the estimation of plant water content of agricultural canopies," *Remote Sens. Environ.*, vol. 87, no. 2-3, pp. 148–160, 2003.

[21] Y. Xie, Z. Sha, and M. Yu, "Remote sensing imagery in vegetation mapping: A review," *J. Plant Ecol.*, vol. 1, no. 1, pp. 9–23, 2008.

[22] B. A. St-Onge and N. Achaichia, "Measuring forest canopy height using a combination of lidar and aerial photography data," *Int. Arch. Photogrammetry Remote Sens. Spatial Inf. Sci.*, vol. 34, no. 3/W4, pp. 131–138, 2001.

[23] M. A. Lefsky et al., "Lidar remote sensing for ecosystem studies: Lidar, an emerging remote sensing technology that directly measures the three-dimensional distribution of plant canopies, can accurately estimate vegetation structural attributes and should be of particular interest to forest, landscape, and global ecologists," *BioScience*, vol. 52, no. 1, pp. 19–30, 2002.

[24] M. A. Wulder et al., "Lidar sampling for large-area forest characterization: A review," *Remote Sens. Environ.*, vol. 121, pp. 196–209, 2012.

[25] G. P. P. Asner et al., "A universal airborne LiDAR approach for tropical forest carbon mapping," *Oecologia*, vol. 168, no. 4, pp. 1147–1160, 2012.

[26] V. Ussyshkin and L. Theriault, "Airborne lidar: Advances in discrete return technology for 3D vegetation mapping," *Remote Sens.*, vol. 3, no. 3, pp. 416–434, 2011.

[27] J. E. Anderson et al., "Integrating waveform lidar with hyperspectral imagery for inventory of a northern temperate forest," *Remote Sens. Environ.*, vol. 112, no. 4, pp. 1856–1870, 2008.

[28] J. T. Mundt, D. R. Streutker, and N. F. Glenn, "Mapping sagebrush distribution using fusion of hyperspectral and lidar classifications," *Photogrammetric Eng. Remote Sens.*, vol. 72, no. 1, pp. 47–54, 2006.

[29] T. T. Sankey et al., "UAV hyperspectral and lidar data and their fusion for arid and semi-arid land vegetation monitoring," *Remote Sens. Ecol. Conservation*, vol. 4, no. 1, pp. 20–33, 2018.

[30] O. Nevalainen et al., "Fast and nondestructive method for leaf level chlorophyll estimation using hyperspectral LiDAR," *Agricultural Forest Meteorol.*, vol. 198, pp. 250–258, 2014.

[31] G. Wei et al., "Multi-wavelength canopy LiDAR for remote sensing of vegetation: Design and system performance," *ISPRS J. Photogrammetry Remote Sens.*, vol. 69, pp. 1–9, 2012.

[32] T. Hakala et al., "Full waveform hyperspectral LiDAR for terrestrial laser scanning," *Opt. Exp.*, vol. 20, no. 7, pp. 7119–7127, 2012.

[33] S. Kaasalainen et al., "Incidence angle dependency of leaf vegetation indices from hyperspectral lidar measurements," *Photogramm. Fernerkundung Geoinform*, vol. 2016, pp. 75–84, 2016.

[34] G. H. Mohammed et al., "Remote sensing of solar-induced chlorophyll fluorescence (SIF) in vegetation: 50 years of progress," *Remote Sens. Environ.*, vol. 231, 2019, Art. no. 111177.

[35] X. Zhao et al., "Active 3D imaging of vegetation based on multi-wavelength fluorescence LiDAR," *Sensors*, vol. 20, no. 3, 2020, Art. no. 935.

[36] X. Wang et al., "Drone-based area scanning of vegetation fluorescence height profiles using a miniaturized hyperspectral lidar system," *Appl. Phys. B*, vol. 124, no. 11, pp. 1–5, 2018.

[37] H. Månefjord, L. Müller, J. Salvador, A. Runemark, C. Kirkeby, and M. Brydegaard, "Low-cost and lightweight hyperspectral lidar for mapping vegetation fluorescence," in *Proc. EPJ Web Conf. ILRC*, 2022, pp. 1–6.

[38] G. Zhao et al., "Inelastic hyperspectral lidar for profiling aquatic ecosystems," *Laser Photon. Rev.*, vol. 10, no. 5, pp. 807–813, 2016.

[39] H. Månefjord et al., "3D-Printed fluorescence hyperspectral lidar for monitoring tagged insects," *IEEE J. Sel. Topics Quantum Electron.*, vol. 28, no. 5, Sep./Oct. 2022, Art. no. 7100109.

[40] G. Zhao et al., "Particle profiling and classification by a dual-band continuous-wave lidar system," *Appl. Opt.*, vol. 57, no. 35 pp. 10164–10171, 2018.

[41] L. Mei and P. P. Guan, "Development of an atmospheric polarization Scheimpflug lidar system based on a time-division multiplexing scheme," *Opt. Lett.*, vol. 42, no. 18, pp. 3562–3565, 2017.

[42] E. Ahokas et al., "Calibration of the Optech ALTM 3100 laser scanner intensity data using brightness targets," *Int. Arch. Photogramm. Remote Sens. Spat. Inf. Sci*, vol. 36, pp. 1–6, 2006.

[43] N. Wang et al., "Diurnal variation of sun-induced chlorophyll fluorescence of agricultural crops observed from a point-based spectrometer on a UAV," *Int. J. Appl. Earth Observation Geoinformation*, vol. 96, 2021, Art. no. 102276.

[44] O. Van Kooten and J. F. Snel, "The use of chlorophyll fluorescence nomenclature in plant stress physiology," *Photosynthesis Res.*, vol. 25, no. 3, pp. 147–150, 1990.

[45] B. Anderson, *Diode Laser Spectroscopic Studies of Biological Materials Using Absorption and Emission Techniques*. Cape Coast, Ghana: Univ. Cape Coast, 2010.

[46] B. Genty, J.-M. Briantais, and N. R. Baker, "The relationship between the quantum yield of photosynthetic electron transport and quenching of chlorophyll fluorescence," *Biochimica et Biophysica Acta (BBA)-Gen. Subjects*, vol. 990, no. 1, pp. 87–92, 1989.

[47] T. Ishida et al., "A novel approach for vegetation classification using UAV-based hyperspectral imaging," *Comput. Electron. Agriculture*, vol. 144, pp. 80–85, 2018.

[48] J. Verrelst et al., "Quantifying vegetation biophysical variables from imaging spectroscopy data: A review on retrieval methods," *Surv. Geophys.*, vol. 40, no. 3, pp. 589–629, 2019.

Rabbi Boateng born in Kumasi, Ghana, in 1995. He received the M.Phil. degree in physics in 2021 from the University of Cape Coast Ghana, Cape Coast, Ghana, where he is currently working toward the Ph.D. degree in physics with the Department of Physics as part of the AFSIN Doctoral Programme with focus on applied fluorescence spectroscopy.

Andrew Atiogbe Huzortey born in Accra, Ghana, in 1990. He received the M.Phil. degree in physics in 2016 from the University of Cape Coast, Cape Coast, Ghana, where he is currently working toward the Ph.D. degree in physics with the Department of Physics with interest in low cost optical spectroscopy applications for health, agriculture and environmental studies.

Yatana Adolphe Gbogbo born in Biankouma, Côte d'Ivoire, in 1987. He received the bachelor's degree in applied and fundamental science and the master's degree in photonics from the University of Nangui Abrogoua, Abidjan, Côte d'Ivoire, in 2015 and 2017, respectively. He is currently working toward the Doctoral degree in entomological remote sensing and spectroscopy with the Department of Applied Electronics and Electricity, National Polytechnic Institute, Yamoussoukro, Côte d'Ivoire.

Assoumou saint-doria Yamoa was born in Agoua, Bongouanou, Côte d'Ivoire, in 1994. He received the bachelor's degree in fundamental and applied sciences and the master's degree in photonics with Nangui Abrogoua University, Abidjan, Côte d'Ivoire, in 2018 and 2020, respectively. He is currently working toward the Doctorate degree in entomological remote sensing and spectroscopy with the Department of Applied Electronics and Electricity, National Polytechnic Institute of Yamoussoukro, Yamoussoukro, Côte d'Ivoire.

Jérémie T. Zoueu received the M.S. degree in laser engineering from the Galilee Institute (University of Paris XIII), Paris, France, in 1992, and the Ph.D. degree in physics from the Pierre and Marie Curie University, Paris, in the field of lasers and photonic materials in 1996. He is currently a Professor of photonics with the National Polytechnic Institute (INP-HB), Yamoussoukro, Cote d'Ivoire. He is currently the Vice President with the University of San-Pedro, San Pedro Sula, Honduras, in charge of the Academic Affairs, and the Founder and the Head of the Laboratory of Instrumentation, Image and Spectroscopy, INP-HB. On the international level, he is the Coordinator of the African Spectral Imaging Network and a Virginia Commonwealth University Affiliate Faculty.

Mikkel Brydegaard born in Copenhagen, Denmark, in 1980. Mikkel received the M.Sc. degree in electrical engineering and the Ph.D. degree in atomic physics, biophotonics and remote sensing from Lund University, Lund, Sweden, in 2007 and 2012, respectively. Mikkel is/was a Postdoctoral Researcher with Stellenbosch University, South Africa and Norsk Elektro Optikk, Oslo, Norway. Mikkel was the recipient of the Inaba prize in 2014, Docent in 2016, and a Senior Lecturer in 2021 with Lund University. Mikkel is/was ERC awardee 2018, and a Co-Founder of the African Spectral Imaging Network and FaunaPhotonics, Denmark.

Benjamin Anderson received the M.Phil. degree from the University of Cape Coast, Cape Coast, Ghana, in 2004, and the Ph.D. degree as a sandwich, between Lund University, Lund, Sweden and the University of Cape Coast, in 2010. Since 2018, he has been an Associate Professor of physics, specifically in applied optics, with the University of Cape Coast. He is currently the Co-Ordinator of the Laser and Fibre Optics Centre, University of Cape Coast, and Ghana's node in African Spectral Imaging Network.

Hampus Månefjord born in Lekeryd, Sweden, in 1992. He received the M.Sc. degree in physics engineering from Lund University, Lund, Sweden, in 2018. Part of the master's degree was completed from Nanyang Technological University, Singapore. He is currently working toward the Ph.D. degree in low-cost optical instrumentation for biophotonics with the Department of Physics, Lund University. He is/was the Swedish research council funds the Ph.D. project to support scientific advancements in low-income regions.